



## Three-dimensionally ordered macroporous PrO<sub>x</sub>: An improved alternative to ceria catalysts for soot combustion

Virginia Alcalde-Santiago, Esther Bailón-García\*, Arantxa Davó-Quiñonero, Dolores Lozano-Castelló, Agustín Bueno-López

*Department of Inorganic Chemistry, University of Alicante, Carretera de San Vicente s/n. E03080, Alicante, Spain*



### ARTICLE INFO

**Keywords:**

Soot  
Praseodymia  
Ceria  
3DOM  
NO<sub>x</sub>

### ABSTRACT

The synthesis and use for soot combustion of praseodymium oxide with three-dimensionally ordered macroporous (3DOM) structure is described. This novel PrO<sub>x</sub>-3DOM catalyst is presented as an improved noble-metal-free alternative to CeO<sub>2</sub> as soot combustion catalyst. The PrO<sub>x</sub>-3DOM catalyst presents a defined 3DOM structure with high macropores volume, which significantly enhances the solid-solid soot-catalyst contact. This enhanced contact, together with the improved reducibility of PrO<sub>x</sub> regarding CeO<sub>2</sub>, ameliorate the active oxygen production and its transfer to soot particles, improving the soot combustion with O<sub>2</sub>. In addition, the higher ability of PrO<sub>x</sub> to oxidize NO to NO<sub>2</sub>, improves the soot combustion in a higher extent than CeO<sub>2</sub> in presence of NO<sub>x</sub>. The catalytic activity of PrO<sub>x</sub>-3DOM after several soot combustion cycles is also confirmed.

### 1. Introduction

The main pollutants emitted by diesel engines are carbon particles and NO<sub>x</sub>, together with certain amounts of CO and hydrocarbons [1,2]. These four compounds are responsible, in part, for the air pollution, and there is a set of requirements that regulate the permissible limits for the emissions of combustion gases from these vehicles [3,4]. In recent years, significant efforts have been made in order to develop new systems to eliminate the carbon particles (soot) emitted by diesel engines, since these particles are responsible for severe environmental and health problems [5,6]. These systems usually consist of a filter placed in the exhaust pipe, where the particles are retained and burned [7–9]. Nevertheless, the temperature of the exhaust gases of modern diesel engines is relatively low (150–500 °C) [10,11] and consequently, is not enough for the spontaneous combustion of soot (550–700 °C) [12]. Thus, a catalyst is required to decrease the combustion temperature of retained particles.

Platinum-based catalysts are the best combustion catalysts in terms of activity and stability for a practical application [13–15]. However, the high cost and limited reserves of Pt are the main barrier for mass commercialization. Other alternative catalysts are being sought to try to improve or, at least, equalize the activity of these platinum catalysts but with lower cost. Cerium oxide is one of the most promising alternative catalysts, since ceria can generate highly reactive oxygen species, which are usually referred to as “active oxygen”. This active oxygen is highly

oxidizing and very efficient for soot combustion [16–19]. Nevertheless, one of the main problems of this active oxygen-reaction pathway is the poor contact between the solid particles of carbon and the solid particles of catalyst. It has been demonstrated by several authors that the use of ceria with a three-dimensional ordered macroporous structure (3DOM) greatly improves the soot combustion due to the improvement of such solid-solid contact [20–24]. 3DOM oxides with large pore sizes (> 50 nm) and interconnected macroporous tunnels permit the accessibility of soot particles to the active sites on the internal surfaces of the catalysts but also make soot particles to transfer easily through the open structure and have less diffusion resistance to reach active sites [25–29].

In addition to the active oxygen mechanism, ceria-catalyzed soot combustion could be also enhanced in presence of NO<sub>x</sub> by the so-called “NO<sub>2</sub>-assisted mechanism” [30]. However, only 5% of the NO<sub>x</sub> present in the exhaust gases is NO<sub>2</sub>, and thus, NO has to be previously oxidized to NO<sub>2</sub> by the catalyst [30]. Ceria catalyzes the oxidation of NO to NO<sub>2</sub> in a certain extent, but the activity is much lower to that of platinum. However, opposite to platinum, NO<sub>2</sub> produced by a ceria catalyst can directly react with soot or can be adsorbed on ceria generating more “active oxygen” by the decomposition of nitrogen-containing groups [31], both reaction pathways improving the soot combustion.

However, despite the wide applicability, pure ceria remains some drawbacks like thermal sintering and deactivation of the redox couple, which result in the decline of oxygen storage/release capability and

\* Corresponding author.

E-mail address: [estherbg@ugr.es](mailto:estherbg@ugr.es) (E. Bailón-García).

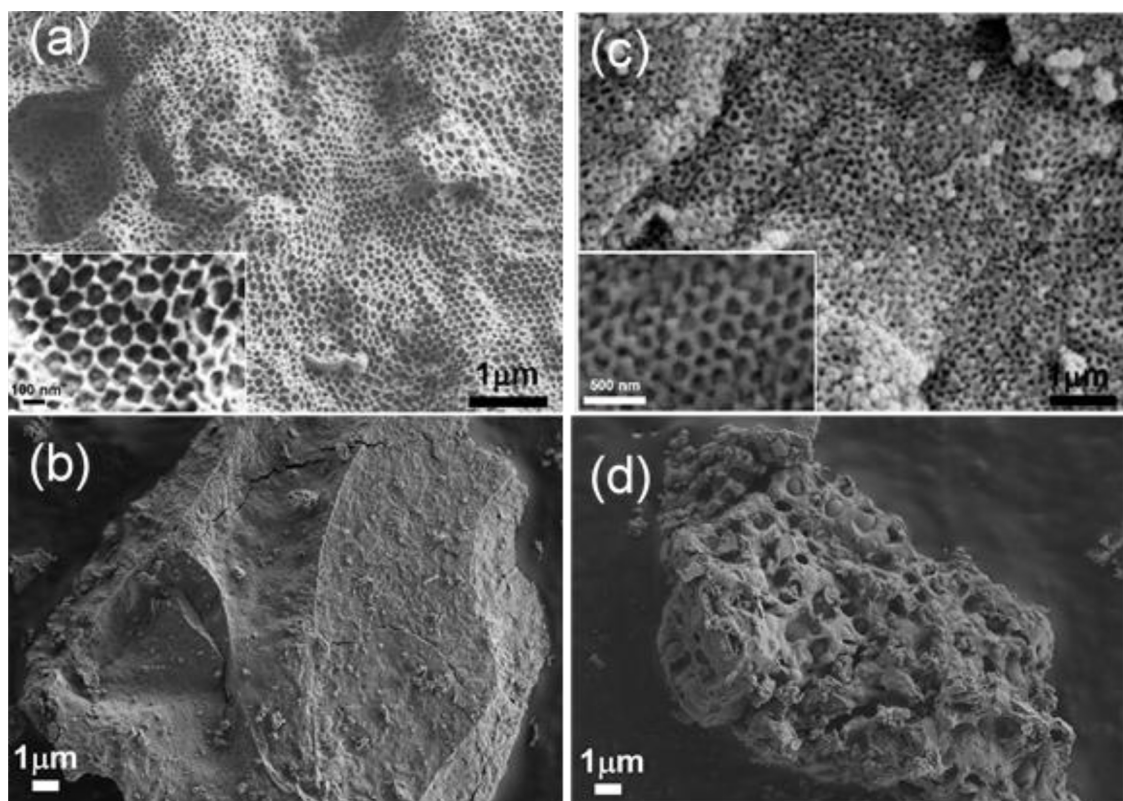


Fig. 1. SEM images of a)  $\text{PrO}_x\text{-3DOM}$ , b)  $\text{PrO}_x\text{-Ref}$ , c)  $\text{CeO}_2\text{-3DOM}$  and d)  $\text{CeO}_2\text{-Ref}$ .

catalytic activity [32]. Several efforts have been made to eliminating these drawbacks of ceria by doping with other isovalent/aliovalent cations such as  $\text{Zr}^{4+}$ ,  $\text{Hf}^{4+}$ ,  $\text{Pr}^{3+}$  or  $\text{La}^{3+}$  [32–34]. In that sense, praseodymium have been mainly studied as a dopant to be introduced into the ceria lattice to enhance the oxygen storage/release capability by creating intrinsic oxygen vacancies thereby increasing the oxygen mobility by facilitating the  $\text{Ce}^{3+}/\text{Ce}^{4+}$  redox process [33].

Praseodymium oxide could be presented as an improved alternative to ceria catalysts because of, akin ceria, can adopt oxygen-deficient stoichiometries, and even, the  $\text{Pr}^{4+}/\text{Pr}^{3+}$  pair has a greater reduction potential than the  $\text{Ce}^{4+}/\text{Ce}^{3+}$  pair, and moreover, presents higher ability for the  $\text{NO}_2$  production [35]. Thus, both mechanisms described for ceria-catalyzed soot combustion could be enhanced in praseodimia catalysts. Herein we describe the synthesis of  $\text{PrO}_x\text{-3DOM}$  and its use, for the first time, in the soot combustion. Its behavior has been compared with that of  $\text{CeO}_2\text{-3DOM}$ , and non-structured  $\text{CeO}_2$  and  $\text{PrO}_x$  catalysts (which are referred to as “Ref” in this article) have been also prepared and tested for comparison.

## 2. Materials and methods

### 2.1. Catalysts preparation

$\text{PrO}_x$  and  $\text{CeO}_2$  catalysts have been prepared with conventional (Ref) and three dimensionally ordered macroporous (3DOM) structures. 3DOM catalysts were synthesized by infiltration of the metal precursor in a polymethylmethacrylate colloidal crystal template, which is then removed by calcination. Briefly, a polymethylmethacrylate (PMMA) colloidal crystals were prepared by polymerization of methylmethacrylate (Sigma Aldrich, 99%), methacrylic acid (Sigma Aldrich, 99%) and divinylbenzene (Sigma Aldrich) (100:1:5 vol ratio) in boiling aqueous solution. Polymerization was conducted for 75 min using potassium persulfate as polymerization initiator. After cooling, the colloidal crystals of PMMA were impregnated with an ethanolic precursor

solution. This solution was prepared dissolving  $\text{M}(\text{NO}_3)_3 \cdot 6\text{H}_2\text{O}$  ( $\text{M}$ : Pr or Ce, Aldrich, 99%) in ethanol (0.476 M) and adding citric acid in stoichiometric proportion to force the precipitation of metal citrates upon solvent evaporation. Afterwards, the solid was calcined at 600 °C for 6 h with a heating rate of 1 °C/min in a muffle furnace under static air to remove the PMMA template. The reference catalysts were prepared following the same procedure but skipping the impregnation step, that is, the dissolution with citric acid and the  $\text{M}$  precursor was directly dried and calcined.

### 2.2. Catalysts characterization

SEM images were obtained in a Field Emission Scanning Electron Microscope (FESEM) Merlin VP Compact from Zeiss, working at very low voltages (from 0.02 kV to 30 kV) to minimize charging effects.

The porosity of catalysts was characterized by  $\text{N}_2$  adsorption, mercury intrusion porosimetry and Helium density.  $\text{N}_2$  adsorption-desorption isotherms were measured at -196 °C in an automatic volumetric system (Autosorb-6, Quantachrome) after degassing the catalysts at 150 °C for 2 h under vacuum. The macroporosity of the catalysts was studied by mercury porosimetry in a Poremaster 60 GT (Quantachrome). The powdered catalysts were outgassed in this case at 50 °C under vacuum for 12 h. The closed porosity was studied by helium pycnometry using an automatic helium pycnometer MicroUltrapyc 1200e (Quantachrome).

X-ray diffractograms were recorded in a Rigaku Miniflex II diffractometer, using  $\text{CuK}\alpha$  radiation ( $\lambda = 0.15418 \text{ nm}$ ). Diffractograms were registered between 10 and 90° ( $2\theta$ ) with a step of 0.025°. The average crystal sizes ( $D$ ) were determined using the equation of Scherrer.

Temperature programmed reduction experiments were carried out with  $\text{H}_2$  ( $\text{H}_2\text{-TPR}$ ) in a thermobalance (Mettler Toledo; TGA/SDTA851) coupled to a mass spectrometer (Pfeiffer Vacuum; Thermostar GSD301 T). The catalysts (20 mg) were heated in 5%  $\text{H}_2/\text{Ar}$  (40 ml/

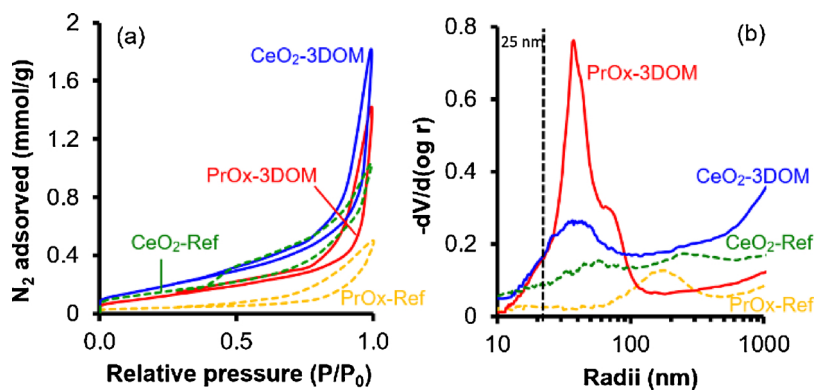


Fig. 2. a) N<sub>2</sub>-adsorption isotherms and b) Pore size distributions determined by mercury intrusion porosimetry.

min) at 10 °C/min from room temperature until 900 °C.

XPS characterization was carried out in a K-ALPHA Thermo Scientific device, using Al-K $\alpha$  radiation (1486.6 eV). The X-ray spot was focussed on the catalysts with a diameter of 400  $\mu$ m, at 3 mA  $\times$  12 kV. The binding energy scale was adjusted by setting the C1s transition at 284.6 eV.

### 2.3. Catalytic tests

Catalytic experiments at programmed temperature (25–700 °C at 10 °C/min) were carried out in a fixed-bed tubular quartz reactor using a mixture of 20 mg of carbon black (Printex U), 80 mg of catalyst and 300 g SiC; prepared with a spatula in the so-called loose-contact mode in order to obtain results with practical meaning. Two gas mixtures were used (500 ml/min; GHSV = 30,000 h<sup>-1</sup>): 5% O<sub>2</sub>/N<sub>2</sub> and 500 ppm NO/5% O<sub>2</sub>/N<sub>2</sub>. The composition of the exhaust gases was controlled by a Specific NDIR-UV gas analyzers for CO, CO<sub>2</sub>, NO, NO<sub>2</sub> and O<sub>2</sub> (Fisher-Rosemount, models BINOS 100, 1001 and 1004).

## 3. Results and discussion

A polymethylmethacrylate colloidal crystal template (PMMA) was synthetized and impregnated with an ethanolic solution of praseodymium or cerium citrate prepared *in situ* by reaction of metal nitrate and citric acid. After template removal by air combustion, high-quality three-dimensional structures were obtained, consisting of an ordered network of macropores with a diameter of 80 nm approximately. This is observed in scanning electron microscopy images (Fig. 1a-b). Defined 3DOM structures are observed for PrO<sub>x</sub>-3DOM and CeO<sub>2</sub>-3DOM while Ref catalysts, obtained by direct calcination of the metal citrates, exhibit closed and compact structures (Fig. 1c-d) with some evidences of gas release during the calcination step in the case of CeO<sub>2</sub>-Ref.

This macroporous character of the 3DOM catalysts was confirmed by N<sub>2</sub>-adsorption and Hg porosimetry (Fig. 2). Type II isotherms,

characteristics of non-porous or macroporous adsorbent, were obtained for all catalysts. However, according with SEM images, significant differences are observed depending on the structure. 3DOM catalysts, as expected, present a strong and fast N<sub>2</sub>-adsorption at high relative pressures denoting the presence of high macropores volume. Both 3DOM catalysts show a well-defined peak in the pore-size distributions obtained by Hg porosimetry for pore radii around 40 nm (Fig. 2b). PrO<sub>x</sub>-3DOM presents the highest macroporous volume because of the better-defined three-dimensional structure.

Higher N<sub>2</sub>-uptake is observed at low relative pressures in CeO<sub>2</sub>-based catalysts regarding PrO<sub>x</sub> ones, denoting the creation of certain microporosity during the gases release. The microporosity contribution to the apparent surface area (S<sub>BET</sub>) is clearly observed in Table 1; higher surface areas were obtained for CeO<sub>2</sub> samples despite the lower macroporosity values.

X-Ray diffractograms (included in the supplementary material file, Figure S1) reveal the stabilization of fluorite-structured cubic CeO<sub>2</sub> (JCPDS 00-034-0394) and Pr<sub>6</sub>O<sub>11</sub> (JCPDS 42-1121), respectively, with fcc unit cells. Significant differences are not observed in d spacing and crystal sizes (Table 1), and consequently, crystallinity is not an important factor to take into account in the activity discussion.

Closed porosity was analyzed by He density measurements (Table 1). In all cases, the He density is lower than the expected value, denoting the existence of closed porosity, which is not accessible neither for He in density measurements nor for N<sub>2</sub> during adsorption-desorption. Note that this difference is more significant in PrO<sub>x</sub> samples. This closed porosity is ascribed, in part, to the presence of carbonates [20–24]. The amount of carbonates determined by XPS is higher in the case of PrO<sub>x</sub> samples (Figure S2 and Table 1) and, either in CeO<sub>2</sub> and PrO<sub>x</sub> catalysts, the carbonates amount decreases in 3DOM samples. These facts could be related to the basicity of the samples. It has been reported that both strength and number of basic sites are higher in Pr<sub>6</sub>O<sub>11</sub> regarding CeO<sub>2</sub> [36–38]. Since CeO<sub>2</sub> has lower basicity than Pr<sub>6</sub>O<sub>11</sub>, it alleviates the possibility of adsorption of CO<sub>2</sub> and the

**Table 1**  
Results of catalysts characterization by N<sub>2</sub> adsorption, helium density, XRD and XPS.

Catalysts	S <sub>BET</sub> (m <sup>2</sup> g <sup>-1</sup> )	$\rho_{\text{He}}^{\text{a}}$ (cm <sup>3</sup> g <sup>-1</sup> )	D <sup>b</sup> (nm)	V <sub>macro</sub> <sup>c</sup> (cm <sup>3</sup> g <sup>-1</sup> )	Carbonates <sup>d</sup> (%)	M <sup>3+</sup> <sup>d</sup> (%)	O <sub>ads</sub> /O <sub>latt</sub> <sup>d</sup>
CeO <sub>2</sub> -Ref	13	6.9 (7.2)	21	0.108	12.1	34.4	0.23
CeO <sub>2</sub> -3DOM	27	6.9 (7.2)	26	0.174	7.7	35.4	0.75
PrO <sub>x</sub> -Ref	3	6.3 (6.9)	26	0.030	22.5	33.5	1.86
PrO <sub>x</sub> -3DOM	10	6.6 (6.9)	26	0.265	20.3	52.6	2.01

<sup>a</sup> He density ( $\rho_{\text{He}}$ ): expected He density values in brackets.

<sup>b</sup> D: crystallite size.

<sup>c</sup> Vmacro: porosity volume up to 100 nm obtained by Hg porosimetry.

<sup>d</sup> Data from XPS analysis (XPS spectra are included in the supplementary material file).

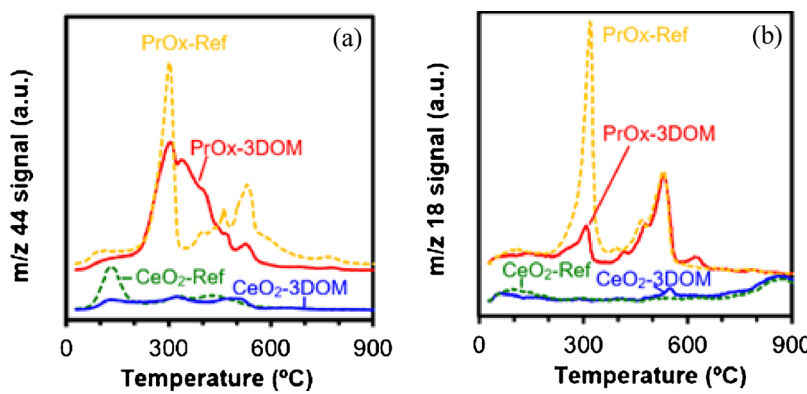


Fig. 3. H<sub>2</sub>-TPR characterization of catalysts: a) CO<sub>2</sub> ( $m/z$  44) and b) H<sub>2</sub>O ( $m/z$  18) signals.

formation of carbonates. Moreover, it has been also reported that the basicity decreases increasing the M<sup>3+</sup> concentration [39–41] and consequently, lower amount of carbonates is detected in 3DOM structures (see M<sup>3+</sup> percentages in Table 1). A surface enrichment of M<sup>3+</sup> ions is observed in 3DOM catalysts in comparison with Ref materials, denoting a surface oxygen deficiency in 3DOM materials. This fact is also corroborated by the higher O<sub>ads</sub>/O<sub>latt</sub> ratio observed in 3DOM samples, since O<sub>ads</sub> species are usually present at the oxygen vacancies and thus, a large amount of O<sub>ads</sub> species implies a higher oxygen vacancy density. This higher surface oxygen vacancies in 3DOM samples could be ascribed to the O<sub>2</sub>-poor environment created during PMMA combustion [42,43]. It is well accepted that the presence of oxygen vacancies is favorable for the improvement in reducibility. Consequently, an improved reducibility could be expected in 3DOM samples and in PrO<sub>x</sub> samples according with the O<sub>ads</sub>/O<sub>latt</sub> ratio (Figure S3 and Table 1).

The reducibility and the presence of carbonates/bicarbonates was

studied by H<sub>2</sub>-TPR (Fig. 3). The CO<sub>2</sub> desorption signal reveals the presence of different amount and strength of basic centres. A CO<sub>2</sub> peak at around 300 °C is obtained for PrO<sub>x</sub> samples, whereas CeO<sub>2</sub> catalysts gave only a small desorption peak at around 120 °C, indicating lower and weaker basicity. In both cases, this peak decreases in 3D-structured samples according with previous observations. The reduction of the catalysts was followed by the  $m/z$  18 signal. As expected, PrO<sub>x</sub> catalysts are reduced at lower temperature and in a higher extent than CeO<sub>2</sub> ones, which is in agreement with the higher reduction potential of the Pr<sup>4+</sup>/Pr<sup>3+</sup> pair. Bulk Pr<sup>4+</sup> is reduced to Pr<sup>3+</sup> between 400–600 °C, whereas bulk Ce<sup>4+</sup> is reduced to Ce<sup>3+</sup> at temperatures higher than 860 °C. Peaks at lower temperatures are observed for 3DOM samples. A peak at around 500 °C appears in CeO<sub>2</sub>, ascribed to surface ceria reduction, and around 250 °C in PrO<sub>x</sub> samples.

This improved reducibility is expected to improve the active oxygen generation and, consequently, the catalytic combustion of soot. This is confirmed in the catalytic experiments performed with O<sub>2</sub>+N<sub>2</sub> (Fig. 4a). In absence of NO<sub>x</sub>, similar catalytic activities were obtained for Ref samples (Fig. 4a) in spite of the different reducibility and oxygen vacancies concentration of both inorganic oxides. Two factors must be considered in the “active oxygen” mechanism: the production of “active oxygen” (affected by the catalyst reducibility) and its transfer from the catalyst surface to the soot particles (affected by the soot-catalyst contact). The limited contact points between soot and catalyst in both Ref samples hinders the active oxygen transfer and, thus, similar activities are obtained in spite of the different active oxygen generation.

The contact is improved by the development of 3DOM structures, improving the combustion activity. Nevertheless, the enhancement is more significant in the PrO<sub>x</sub>-3DOM sample, which can be explained on the base of the better redox properties of this oxide and its well-developed 3DOM structure. PrO<sub>x</sub>-3DOM presents lower BET surface area than CeO<sub>2</sub>-3DOM and worst catalytic performance could be expected in

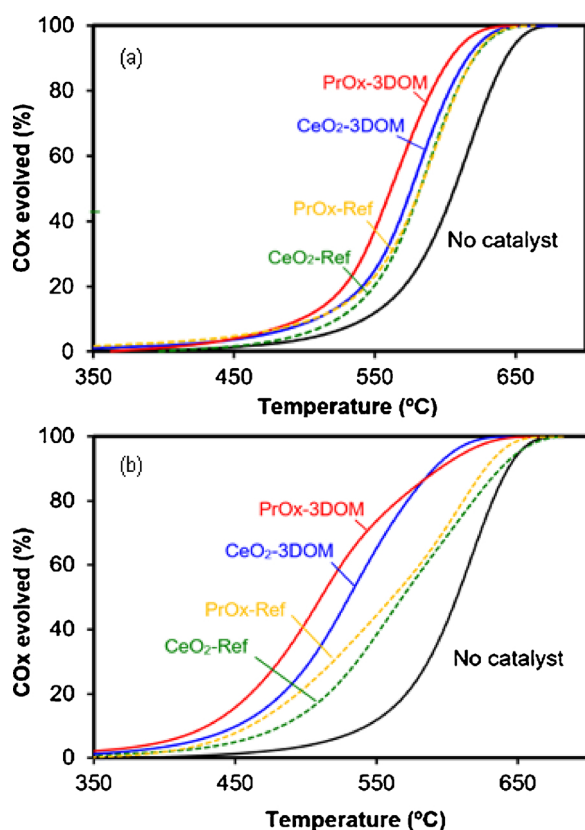


Fig. 4. Soot combustion experiments with (a) 5% O<sub>2</sub> + N<sub>2</sub> and (b) 500 ppm NO<sub>x</sub> + 5% O<sub>2</sub> + N<sub>2</sub>.

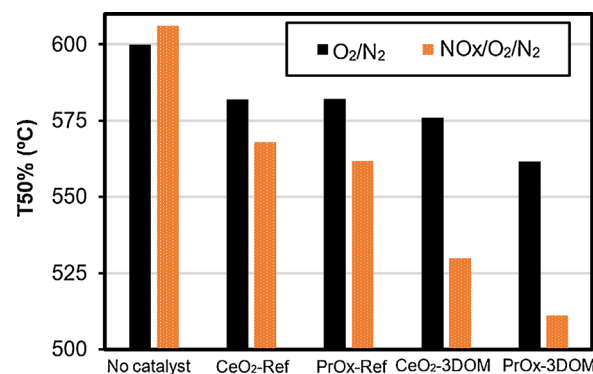


Fig. 5. Comparison of soot combustion in the absence and presence of NO<sub>x</sub>. T50% is the temperature where 50% of soot is oxidised in experiments shown in Fig. 4).

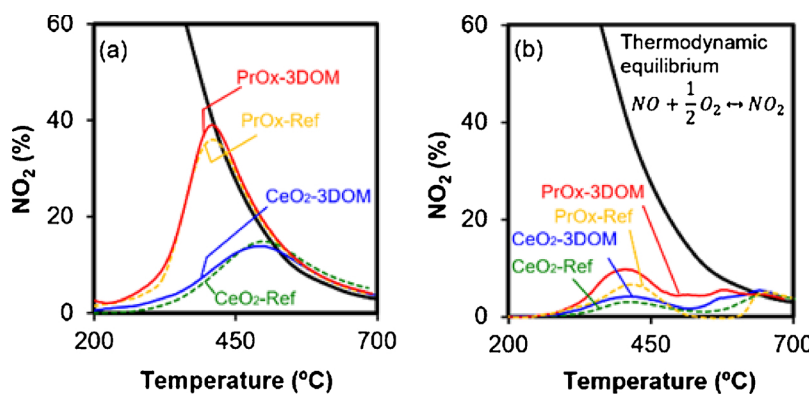


Fig. 6. NO oxidation to NO<sub>2</sub> in catalytic experiments performed (a) without soot and (b) with soot.

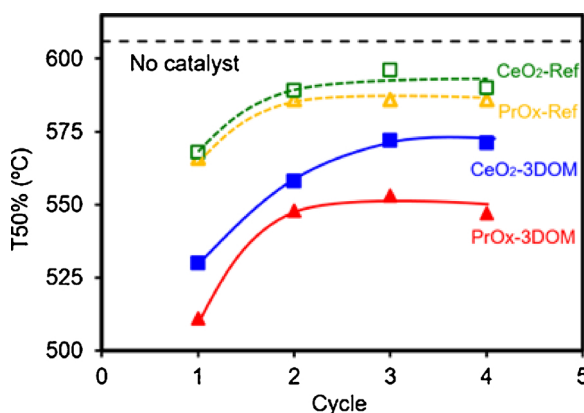


Fig. 7. T50% for consecutive soot combustion cycles performed with 500 ppm NO<sub>x</sub> + 5% O<sub>2</sub> + N<sub>2</sub>.

the former. However, not only surface area is important, the pore size distribution and, thus the accessibility of soot to this surface area is a critical factor to take into account. According to N<sub>2</sub>-isotherms and Hg porosimetry (Fig. 2), CeO<sub>2</sub>-3DOM provides higher porosity in the microporosity and mesoporosity range, while in PrO<sub>x</sub>-3DOM higher volume of macropores is obtained and consequently, despite the lower surface area, the real surface area accessible to soot is improved in the PrO<sub>x</sub>-3DOM sample.

A considerable activity enhancement is observed in presence of NO<sub>x</sub> for all catalysts (see Figs. 4 and 5). A significant decrease of the temperature for 50% soot combustion (T50%) is observed in presence of NO<sub>x</sub> (Fig. 5), and this decrease is higher in PrO<sub>x</sub> catalysts, especially in the case of PrO<sub>x</sub>-3DOM. The 3DOM structure also has an important role in this improvement.

Here, the ability of catalysts to oxidize NO to NO<sub>2</sub> (Fig. 6a) has to be taken into account [35,44]. The catalytic activity for NO oxidation to NO<sub>2</sub> is higher for PrO<sub>x</sub> catalysts, and the 3DOM structure do not affects significantly to this oxidation. The H<sub>2</sub>-TPR of the CeO<sub>2</sub> and PrO<sub>x</sub> catalysts show that the PrO<sub>x</sub> catalysts can be easily reduced (surface and bulk) compared with the CeO<sub>2</sub>. This improvement in the oxidation properties can be correlated to the ‘active oxygen’, which can be easily transferred to the gas-phase NO. Consequently, PrO<sub>x</sub> easily loses the oxygen at the relatively low temperatures and that could be responsible for the enhanced NO conversion into NO<sub>2</sub>. NO<sub>2</sub>, once produced by the catalysts, reacts with soot, as confirmed comparing Figs. 6a and b, where the NO<sub>2</sub> profiles obtained in catalytic experiments without and with soot, respectively, are compiled. PrO<sub>x</sub> catalysts are more efficient in the combustion of soot in presence of NO<sub>x</sub> due to their higher ability to oxidize NO to NO<sub>2</sub>.

Regarding the effect of the 3DOM structure in soot combustion with NO<sub>x</sub> + O<sub>2</sub> + N<sub>2</sub>, the explanation is more complex, since the structure

does not affect NO<sub>2</sub> production. The 3DOM structure improves the soot-catalyst contact, and therefore, the active-oxygen mechanism is more efficient. NO<sub>2</sub> contributes to the creation of active oxygen, together with O<sub>2</sub>. NO<sub>2</sub>, once produced by the catalyst, can either travel in the gas phase and react directly with soot or can be re-adsorbed on the catalyst surface yielding NO and active oxygen [20]. Thus, NO<sub>2</sub> is an efficient way not only for direct soot oxidation but also for active oxygen production, and that is why the 3DOM structure is very positive for soot combustion also in the presence of NO<sub>x</sub>, because NO<sub>2</sub> improves the active oxygen production and the 3DOM structure improves the transfer of active oxygen from catalyst to soot.

The catalysts deactivation after consecutive soot combustion cycles was also evaluated and results are collected in Fig. 7. A loss of activity is observed in all catalysts after the first combustion cycle, either for Ref and 3DOM catalysts. Nevertheless, once the activity is stable, PrO<sub>x</sub>-3DOM keeps better activity than CeO<sub>2</sub>-3DOM, and this is a promising result for the practical utilization of this novel material.

The activity decrease of ceria catalysts during soot combustion experiments has been already reported, and two arguments can be appealed to explain this partial decrease. It is known that pure ceria sinters at high temperature [30], and this could partially explain the activity decrease observed in Fig. 7. In addition, it is known that the catalytic oxidation of NO to NO<sub>2</sub> is an important step in the catalytic oxidation of soot, and this oxidation can involve both hydroxyls groups and surface oxygens on the ceria catalyst [45]. Modifications in this surface chemistry could also explain the partial decrease of the catalytic activity on consecutive soot combustion cycles.

#### 4. Conclusions

In summary, it is reported the synthesis and use for soot combustion, for the first time, of three-dimensionally ordered macroporous PrO<sub>x</sub>. From all the above results and discussion, the following conclusions can be drawn:

- i) A defined macroporous structure with a high volume of macropores has been obtained in the PrO<sub>x</sub>-3DOM catalyst, which significantly enhances the catalyst-soot contact and thus, the activity.
- ii) PrO<sub>x</sub> is more easily reducible than CeO<sub>2</sub>, and the 3DOM structure favors additionally that reducibility.
- iii) PrO<sub>x</sub> presents higher ability to oxidize NO to NO<sub>2</sub> than CeO<sub>2</sub>, which participates in the generation of active oxygen favoring the soot combustion in higher extend.

Consequently, three-dimensionally ordered macroporous PrO<sub>x</sub> presents an improved behaviour to generate active oxygen and to transfer it to soot, which provide an improved performance for the soot combustion with regard to ceria.

## Acknowledgements

The authors thank the financial support of the Spanish Ministry of Economy and Competitiveness (Project CTQ2015-67597-C2-2-R and grant FJCI-2015-23769), the Spanish Ministry of Education, Culture and Sports (grant FPU14/01178) and the UE (FEDER funding).

## Appendix A. Supplementary data

Supplementary material related to this article can be found, in the online version, at doi:<https://doi.org/10.1016/j.apcatb.2018.10.049>.

## References

- [1] M. Fiebig, A. Wiartalla, B. Holderbaum, S. Kiesow, Particulate emissions from diesel engines: correlation between engine technology and emissions, *J. Occup. Med. Toxicol.* 9 (2014) 6, <https://doi.org/10.1186/1745-6673-9-6>.
- [2] I.A. Resitoglu, K. Altinisik, A. Keskin, The pollutant emissions from diesel-engine vehicles and exhaust aftertreatment systems, *Clean Technol. Environ. Policy* 17 (2015) 15–27, <https://doi.org/10.1007/s10098-014-0793-9>.
- [3] T. Germanova, A. Kernozhitskaya, Emissions of exhaust gases and health of the person, *IOP Conf. Ser. Earth Environ. Sci.* 90 (2017) 012036–012040.
- [4] K. Kuklinska, L. Wolska, J. Namiesnik, Air quality policy in the U.S. And the EU – a review, *Atmos. Pollut. Res.* 6 (2015) 129–137, <https://doi.org/10.5094/APR.2015.015>.
- [5] R.O. McClellan, T.W. Hesterberg, J.C. Wall, Evaluation of carcinogenic hazard of diesel engine exhaust needs to consider revolutionary changes in diesel technology, *Regul. Toxicol. Pharmacol.* 63 (2012) 225–258, <https://doi.org/10.1016/j.yrtph.2012.04.005>.
- [6] H. Burtscher, Physical characterization of particulate emissions from diesel engines : a review, *Aerosol Sci.* 36 (2005) 896–932, <https://doi.org/10.1016/j.jaerosci.2004.12.001>.
- [7] D. Fino, V. Specchia, Open issues in oxidative catalysis for diesel particulate abatement, *Powder Technol.* 180 (2008) 64–73, <https://doi.org/10.1016/j.powtec.2007.03.021>.
- [8] B.A.A.L. van Setten, M. Makkee, J.A. Moulijn, Science and technology of catalytic diesel particulate filters, *Catal. Rev.* 43 (2001) 489–564, <https://doi.org/10.1081/CR-120001810>.
- [9] J.P.A. Neef, M. Makkee, J.A. Moulijn, Diesel particulate emission control, *Fuel Process. Technol.* 47 (1996) 1–69, [https://doi.org/10.1016/0378-3820\(96\)01002-8](https://doi.org/10.1016/0378-3820(96)01002-8).
- [10] R. Ramdas, E. Nowicka, R. Jenkins, D. Sellick, C. Davies, S. Golunski, Using real particulate matter to evaluate combustion catalysts for direct regeneration of diesel soot filters, *Appl. Catal. B Environ.* 176–177 (2015) 436–443, <https://doi.org/10.1016/j.apcatb.2015.04.031>.
- [11] M. Bender, S. Unverricht, *Catalytic Conversion of Fuel and Converter Therefor*, US 2002/0083699, 2002.
- [12] N. Russo, D. Fino, G. Saracco, V. Specchia, Studies on the redox properties of chromite perovskite catalysts for soot combustion, *J. Catal.* 229 (2005) 459–469, <https://doi.org/10.1016/j.jcat.2004.11.025>.
- [13] S.J. Jelles, R.R. Krul, M. Makkee, J.A. Moulijn, The influence of NOx on the oxidation of metal activated diesel soot, *Catal. Today* 53 (1999) 623–630, [https://doi.org/10.1016/S0920-5861\(99\)00150-9](https://doi.org/10.1016/S0920-5861(99)00150-9).
- [14] J.O. Uchisawa, A. Obuchi, Z. Zhao, S. Kushiyama, Carbon oxidation with platinum supported catalysts, *Appl. Catal. B Environ.* 18 (1998) L183–L187, [https://doi.org/10.1016/S0926-3373\(98\)00046-0](https://doi.org/10.1016/S0926-3373(98)00046-0).
- [15] G. Neri, L. Bonacorsi, A. Donato, C. Milone, M.G. Musolino, A.M. Visco, Catalytic combustion of diesel soot over metal oxide catalysts, *Appl. Catal. B Environ.* 11 (1997) 217–231, [https://doi.org/10.1016/S0926-3373\(96\)00045-8](https://doi.org/10.1016/S0926-3373(96)00045-8).
- [16] B.M. Reddy, P. Bharali, G. Thrimurthulu, P. Saikia, L. Katta, S.-E. Park, Catalytic efficiency of Ceria-Zirconia and Ceria-Hafnia nanocomposite oxides for soot oxidation, *Catal. Lett.* 123 (2008) 327–333, <https://doi.org/10.1007/s10562-008-9427-3>.
- [17] A. Bueno-López, K. Krishna, M. Makkee, J.A. Moulijn, Enhanced soot oxidation by lattice oxygen via La<sub>3+</sub>-doped CeO<sub>2</sub>, *J. Catal.* 230 (2005) 237–248, <https://doi.org/10.1016/j.jcat.2004.11.027>.
- [18] E. Aneggi, C. de Leitenburg, G. Dolcetti, A. Trovarelli, Promotional effect of rare earths and transition metals in the combustion of diesel soot over CeO<sub>2</sub> and Ce<sub>0.2</sub>ZrO<sub>2</sub>, *Catal. Today* 114 (2006) 40–47, <https://doi.org/10.1016/j.cattod.2006.02.008>.
- [19] J. Lahaye, S. Boehm, P. Chambrion, P. Ehrburger, Influence of cerium oxide on the formation and oxidation of soot, *Combust. Flame* 104 (1996) 199–207, [https://doi.org/10.1016/0010-2180\(95\)00176-X](https://doi.org/10.1016/0010-2180(95)00176-X).
- [20] V. Alcalde-Santiago, A. Davó-Quiñonero, D. Lozano-Castelló, A. Bueno-López, On the soot combustion mechanism using 3DOM ceria catalysts, *Appl. Catal. B Environ.* 234 (2018) 187–197, <https://doi.org/10.1016/j.apcatb.2018.04.023>.
- [21] J. Wang, L. Cheng, W. An, J. Xu, Y. Men, Boosting soot combustion efficiencies over Cu<sub>0.2</sub>CeO<sub>2</sub> catalysts with a 3DOM structure, *Catal. Sci. Technol.* 6 (2016) 7342–7350, <https://doi.org/10.1039/C6CY01366J>.
- [22] Y. Wei, J. Liu, Z. Zhao, A. Duan, G. Jiang, C. Xu, J. Gao, H. He, X. Wang, Three-dimensionally ordered macroporous Ce<sub>0.8</sub>Zr<sub>0.2</sub>O<sub>2</sub>-supported gold nanoparticles: synthesis with controllable size and super-catalytic performance for soot oxidation, *Energy Environ. Sci.* 4 (2011) 2959–2970, <https://doi.org/10.1039/C0EE00813C>.
- [23] G. Zhang, Z. Zhao, J. Liu, G. Jiang, A. Duan, J. Zheng, S. Chen, R. Zhou, Three dimensionally ordered macroporous Ce<sub>1-x</sub>ZrxO<sub>2</sub> solid solutions for diesel soot combustion, *Chem. Commun.* 46 (2010) 457–459, <https://doi.org/10.1039/B915027G>.
- [24] G. Zhang, Z. Zhao, J. Xu, J. Zheng, J. Liu, G. Jiang, A. Duan, H. He, Comparative study on the preparation, characterization and catalytic performances of 3DOM Ce-based materials for the combustion of diesel soot, *Appl. Catal. B Environ.* 107 (2011) 302–315, <https://doi.org/10.1016/j.apcatb.2011.07.029>.
- [25] Y. Wei, Q. Wu, J. Xiong, J. Liu, Z. Zhao, Fabrication of ultrafine Pd nanoparticles on 3D ordered macroporous TiO<sub>2</sub>for enhanced catalytic activity during diesel soot combustion, *Chinese J. Catal.* 39 (2018) 606–612, [https://doi.org/10.1016/S1872-2067\(17\)62939-5](https://doi.org/10.1016/S1872-2067(17)62939-5).
- [26] J. Tan, Y. Wei, Y. Sun, J. Liu, Z. Zhao, W. Song, J. Li, X. Zhang, Simultaneous removal of NOx and soot particulates from diesel engine exhaust by 3DOM Fe-Mn oxide catalysts, *J. Ind. Eng. Chem.* 63 (2018) 84–94, <https://doi.org/10.1016/j.jiec.2018.02.002>.
- [27] C. Rao, R. Liu, X. Feng, J. Shen, H. Peng, X. Xu, X. Fang, J. Liu, X. Wang, Three-dimensionally ordered macroporous SnO<sub>2</sub>-based solid solution catalysts for effective soot oxidation, *Chin. J. Catal.* 39 (2018) 1683–1694, [https://doi.org/10.1016/S1872-2067\(18\)63123-7](https://doi.org/10.1016/S1872-2067(18)63123-7).
- [28] Y. Wei, Z. Zhao, J. Liu, S. Liu, C. Xu, A. Duan, G. Jiang, Multifunctional catalysts of three-dimensionally ordered macroporous oxide-supported Au@Pt core-shell nanoparticles with high catalytic activity and stability for soot oxidation, *J. Catal.* 317 (2014) 62–74, <https://doi.org/10.1016/j.jcat.2014.05.014>.
- [29] B. Jin, X. Wu, D. Weng, S. Liu, T. Yu, Z. Zhao, Y. Wei, Roles of cobalt and cerium species in three-dimensionally ordered macroporous CoxCe<sub>1-x</sub>O<sub>8</sub>catalysts for the catalytic oxidation of diesel soot, *J. Colloid Interface Sci.* 532 (2018) 579–587, <https://doi.org/10.1016/j.jcis.2018.08.018>.
- [30] A. Bueno-López, Diesel soot combustion ceria catalysts, *Appl. Catal. B Environ.* 146 (2014) 1–11, <https://doi.org/10.1016/j.apcatb.2013.02.033>.
- [31] I. Atribak, F.E. López-Suárez, A. Bueno-López, A. García-García, New insights into the performance of ceria-zirconia mixed oxides as soot combustion catalysts. Identification of the role of “active oxygen” production, *Catal. Today* 176 (2011) 404–408, <https://doi.org/10.1016/j.cattod.2010.11.023>.
- [32] B.M. Reddy, G. Thrimurthulu, L. Katta, S. Park, Structural characteristics and catalytic activity of nanocrystalline Ceria - praseodymia solid solutions, *J. Phys. Chem. C* 113 (2009) 15882–15890.
- [33] B.M. Reddy, G. Thrimurthulu, L. Katta, Design of efficient Ce<sub>x</sub>M<sub>1-x</sub>O<sub>2-δ</sub> (M = Zr, Hf, Tb and Pr) nanosized model solid solutions for CO oxidation, *Catal. Letters* 141 (2011) 572–581, <https://doi.org/10.1007/s10562-010-0484-z>.
- [34] G. Thrimurthulu, K.N. Rao, D. Devaiah, B.M. Reddy, Nanocrystalline ceria-praseodymia and ceria-zirconia solid solutions for soot oxidation, *Res. Chem. Intermed.* 38 (2012) 1847–1855, <https://doi.org/10.1007/s11164-012-0508-y>.
- [35] N. Guillén-Hurtado, F.E. López-Suárez, A. Bueno-López, A. García-García, Behavior of different soot combustion catalysts under NO<sub>x</sub>/O<sub>2</sub>. Importance of the catalyst-soot contact, *React. Kinet. Mech. Catal.* 111 (2014) 167–182, <https://doi.org/10.1007/s11144-013-0644-4>.
- [36] M. Itoh, K. Motoki, M. Saito, J. Iwamoto, K. Machida, Lean NO<sub>x</sub> reduction by hydrogen over Pt-Supported rare earth oxide catalysts and their in situ DRIFTS study, *Bull. Chem. Soc. Jpn.* 82 (2009) 1197–1202.
- [37] A.M. Maitra, Determination of solid state basicity of rare earth oxides by thermal analysis of their carbonates, *J. Therm. Anal.* 36 (1990) 657–675, <https://doi.org/10.1007/BF01914518>.
- [38] S. Sato, R. Takahashi, T. Sodesawa, A. Igarashi, H. Inoue, Catalytic reaction of 1,3-butanediol over rare earth oxides, *Appl. Catal. A Gen.* 328 (2007) 109–116, <https://doi.org/10.1016/j.apcata.2007.05.033>.
- [39] B.M.E. Russelbladt, W.F. Hoelderich, New rare earth oxide catalysts for the transesterification of triglycerides with methanol resulting in biodiesel and pure glycerol, *J. Catal.* 271 (2010) 290–304, <https://doi.org/10.1016/j.jcat.2010.02.005>.
- [40] A. Herrmann, H.A. Othman, A.A. Assadi, M. Tiegel, S. Kuhn, C. Rüssel, Spectroscopic properties of cerium-doped aluminosilicate glasses, *Opt. Mater. Express* 5 (2015) 720–732, <https://doi.org/10.1364/OME.5.000720>.
- [41] D. Terribile, A. Trovarelli, J. Llorca, C. de Leitenburg, G. Dolcetti, The synthesis and characterization of mesoporous high-surface area Ceria prepared using a hybrid Organic/Inorganic route, *J. Catal.* 178 (1998) 299–308, <https://doi.org/10.1006/jcat.1998.2152>.
- [42] A. Davó-Quiñonero, J. González-Mira, I. Such-Basañez, J. Juan-Juan, D. Lozano-Castelló, A. Bueno-López, Improved CO oxidation activity of 3DOM Pr-doped ceria catalysts: something other than an ordered macroporous structure, *Catalysts* 7 (2017) 67, <https://doi.org/10.3390/catal7020067>.
- [43] A. Davó-Quiñonero, J. González-Mira, D. Lozano-Castelló, A. Bueno-López, Templated synthesis of Pr-doped ceria with improved micro and mesoporosity porosity, redox properties and catalytic activity, *Catal. Letters* 148 (2018) 258–266, <https://doi.org/10.1007/s10562-017-2215-1>.
- [44] K. Krishna, A. Bueno-López, M. Makkee, J.A. Moulijn, Potential rare-earth modified CeO<sub>2</sub> catalysts for soot oxidation. Part III. Effect of dopant loading and calcination temperature on catalytic activity with O<sub>2</sub> and NO + O<sub>2</sub>, *Appl. Catal. B Environ.* 75 (2007) 210–220, <https://doi.org/10.1016/j.apcatb.2007.04.009>.
- [45] I. Atribak, B. Azambre, A.B. López, A. García-García, Effect of NO<sub>x</sub> adsorption/desorption over ceria-zirconia catalysts on the catalytic combustion of model soot, *Appl. Catal. B Environ.* 92 (2009) 126–137, <https://doi.org/10.1016/j.apcatb.2009.07.015>.